Folding DNA into origami nanostructures enhances resistance to ionizing radiation

Leo Sala,[a] Agnes Zerolová,[a,b] Alvaro Rodriguez,[a] Dan Reimitz,[a] Marie Davídková,[c] Kenny Ebel,[d] Ilko Bald,[d] and Jaroslav Kočišek*[a]

Supplementary Information

1 Procedure for strand break estimation from AGE profiles

1.1 Single-stranded DNA

Based on AGE results, the single-stranded scaffold of the triangles appears to be fragmented by irradiation (Fig. 3 of the main text). At low absorbed doses, the intense band of the intact scaffold is still apparent with the absorbed dose-dependent broadening of a tailing band which is most likely composed of scaffold fragments.[1] Above 50 Gy, the band corresponding to the intact scaffold is already significantly blurred and replaced by the broad band of the scaffold fragments. The intensities are normalized to the sum of the band intensities corresponding to the intact scaffold (I_S) and the fragments (I_{SF}), assuming the same dye-sensitivities for both bands (Equation 1).

Plotting the normalized band intensities with absorbed dose, the fragmentation of the scaffold strand component can then be monitored. We observe exponential decreases of the band related to the intact scaffold ($I_{S,norm}$) with absorbed dose (D). A simple exponential fit (for plots in Fig. 2 of the main text) was utilized to trace the absorbed dose-dependent damage and the number of strand breaks molecule^{-1} Gy^{-1} (μ_{SB}) can be estimated from the decay rate of the scaffold intensity (Equation 2), where I_0 is the $I_{S,norm}$ value for the non-irradiated control sample. As $I_{S,norm}$ is proportional to the number of intact scaffold strands, the exponent μ_{SB}D describes the nicking dose or the average nicks per molecule in time in statistically independent nicking events (Poisson process).[2]

$$I_{S,norm} = \frac{I_S}{I_S + I_{SF}} \tag{1}$$

$$I_{S,norm} = I_0 e^{-\mu_{SB} D} \tag{2}$$

1.2 Double-stranded DNA

For ds-m13mp18, the intensities corresponding to the bands of supercoiled (S), relaxed (R), linear (L) plasmid forms were extracted from the gel profiles and fitted using the Cowan model (Equations 3-5)[2,3] implemented in Python. The parameters μ and ϕ correspond to the estimated rates of single and double strand breaks, respectively, with μ_0 and ϕ_0 corresponding to the strand breaks already present in the unirradiated sample.

$$S = e^{-(\mu_0 + \phi_0 + \mu D + \phi D)} \tag{3}$$

[a] J. Heyrovský Institute of Physical Chemistry of the CAS, Dolejškova 3, 18223 Prague, Czech Republic.
Fax: +420 26605 3910; Tel: +420 26605 2011; E-mail: jaroslav.kocisek@jh-inst.cas.cz
[b] Department of Chemistry, Technical University of Liberec, 46117, Liberec, Czech Republic.
[c] Department of Radiation Dosimetry, Nuclear Physics Institute of the CAS, Na Truhlářce 39/64, 180 00 Prague, Czech Republic.
[d] Institute of Chemistry—Physical Chemistry, Universität Potsdam, Karl-Liebknecht-Straße 24-25, D-14476 Potsdam, Germany.

$$R = (1 - e^{-(\mu_0 + \mu D)})e^{-(\phi_0 + \phi D)} \quad (4)$$

$$L = (\phi_0 + \phi D)e^{-(\phi_0 + \phi D)} \quad (5)$$

Heavy fragmentation is already observed at 50 Gy for the irradiated ds-m13mp18 in H_2O (Fig. S1) so the fitting was limited to 20 Gy. For ds-m13mp18 in 1 mM tris, this fragmentation is starting to be apparent at 100 Gy so the fitting was constrained to 50 Gy. The results are shown in Fig. S1. There appears to be a 13 % reduction in SSB rate and 55 % reduction in DSB rate with increase in tris concentration. The total strand breaks are an order of magnitude greater than those estimated for irradiated DNA origami triangles and ss-m13mp18.

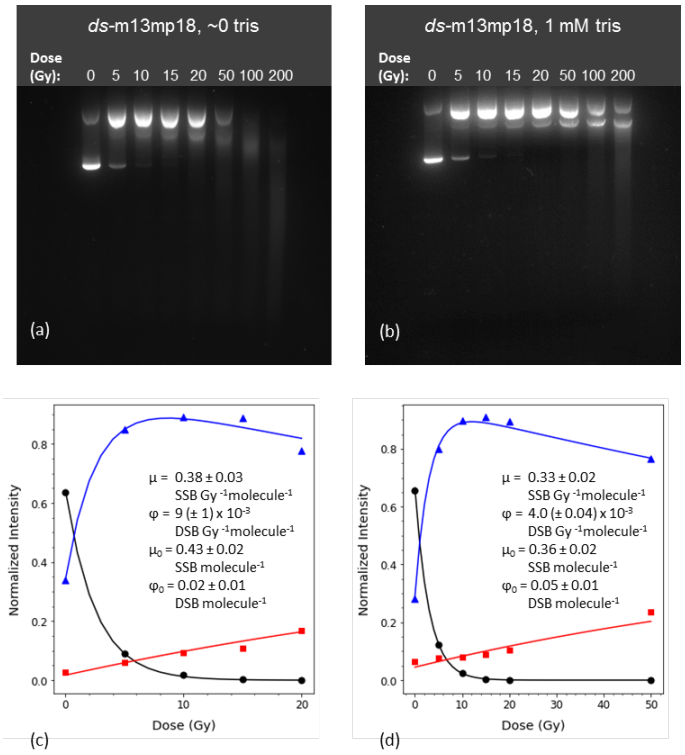

Figure S1 Gel electrophoresis results of gamma-irradiated ds-m13mp18 plasmid DNA in H_2O (a) and in 1 mM tris (b) in 0.8 % gel run for 120 min at 100 V. The results of the Cowan fit on the normalized intensities of supercoiled (circles), relaxed (triangles), and linear (squares) forms are shown in (c) and (d), respectively, for gamma-irradiated ds-m13mp18 in H_2O and 1 mM tris with the resulting fitting parameters.

2 AGE band identification

Fig. S2 shows the electrophoresis results of gamma-irradiated DNA origami nanostructures in low-magnesium, low-tris solutions (lanes 1-8) run alongside intact and irradiated scaffold (lanes 9&10), a concentrated solution of staple strands (lane 11) as well as triangles in folding buffer (1XTAE) denatured by heating to 80°C for 4 min and cooled rapidly by immersion in ice bath (lane 12). The bright high mobility bands are unambiguously coming from staple solutions. The slower bands in irradiated low-magnesium solutions are within the region of the band mobility of the scaffold and denatured triangles in folding buffer although the slight changes in mobility may be caused by the (1) differences in buffer conditions and (2) only partial denaturation of heated triangles as evidenced by the fainter staple-DNA band. To be sure, we run electrophoresis on DNA origami in folding buffer without any treatment and those in H_2O with and without irradiation (Fig. S3). In 10mM Tris, the bands corresponding to intact nanostructures can be observed while in pure water, we can see more mobile bands which can be assigned to the scaffold strand.

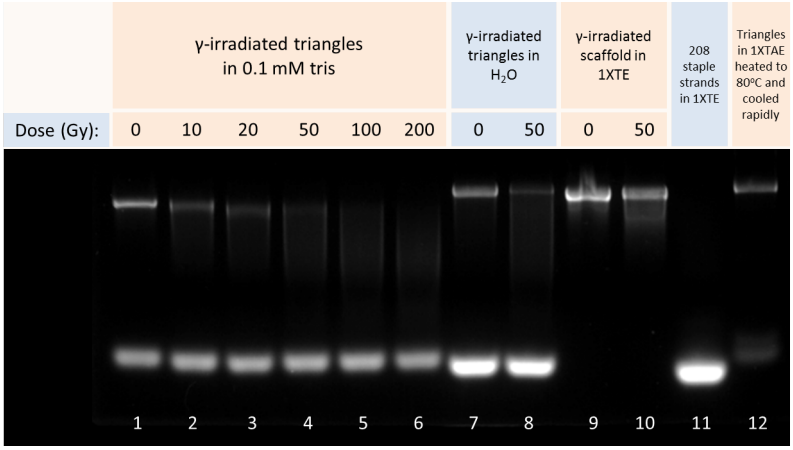

Figure S2 Gel images from the electrophoresis (100 V, 35 min, 1 % agarose) of gamma-irradiated solutions of DNA origami nanostructures in 0.1 mM tris (0-200 Gy, 330 ng DNA lane-1, lanes 1-6), in H_2O (0-50 Gy, 400 ng lane-1, lanes 7-8), gamma-irradiated solutions of scaffold DNA (360 ng lane-1, lanes 9-10), solution of 208 staple strands (∼1000 ng $lane^{-1}$, lane 11), and solution of thermally denatured triangles, heated to 80oC for 4 min and rapidly cooled by immersion in an ice bath (300 ng $lane^{-1}$, lane 12).

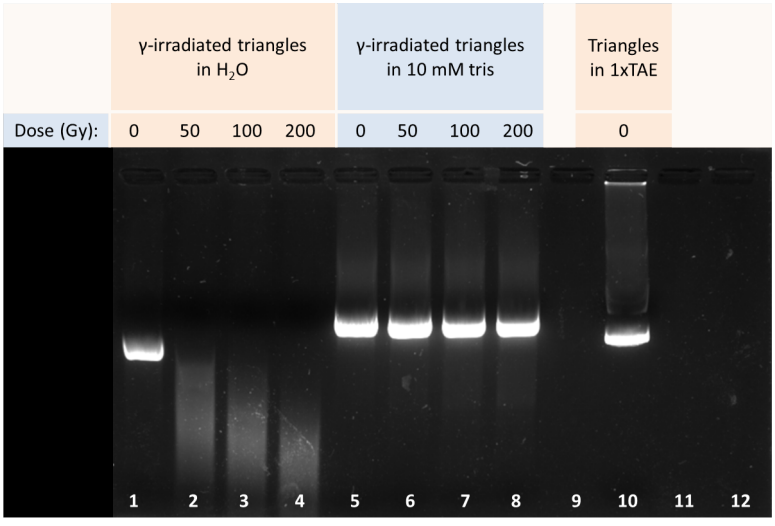

Figure S3 Gel images from the electrophoresis (100 V, 60 min, 1% agarose) of gamma-irradiated solutions of DNA origami nanostructures in H_2O, 10 mM tris with unirradiated DNA origami in folding buffer as reference.

3 Limitations of AGE due to incomplete denaturation

The direct loading of irradiated samples is employed here to avoid subjecting the samples into denaturing conditions that may amplify the radiation-induced damage in solution but it heavily relies on scaffold-staple separation to quantify the damage. Consequently, in high tris concentrations, this scaffold-staple separation in direct electrophoresis in TAE does not occur with a possible transition at around 1 mM tris where the electrophoresis profiles deviate from those observed at low ($<$ 1 mM, with effective scaffold separation) and high ($>$ 1mM, without scaffold separation) tris concentrations causing exceptionally wide error bars for this data set and the sudden drop in the decay rate at this tris concentration (Fig. S4, and Table S1). It is unclear how the pH changes in gamma radiolysis of water and subsequently, DNA solutions with extremely low to no buffering capacity. However, the shape and packing of the triangles have been shown to be sensitive to pH changes[4,5] and this might have caused irregular gel profiles in between irradiations in 1 mM tris.

Solutions with high tris concentrations were nonetheless subjected to denaturing conditions to have an idea of the damages in the DNA origami scaffold that could not be separated by conventional AGE. Here we added enough 0.5xTAE to arrive at a concentration of more than 2x tris:Mg^{2+} into the gamma irradiated triangle solutions to fully chelate the available Mg^{2+} in folding buffer and in 10mM tris. The results are shown in Fig. S5. In this case the separated scaffold is probably in a more linear or relaxed state due to its reduced mobility compared to the intact triangle but this needs further investigation to ascertain. Nevertheless, we can surmise that in the folding buffer, the damage is still undetectable even when the nanostructures are denatured while for 10 mM tris, there appears to be a about 50 % reduction in the scaffold strand band intensity (est. 3 x 10^{-3} strand breaks Gy^{-1} $molecule^{-1}$) at 200 Gy lost to fragments (Fig. S5).

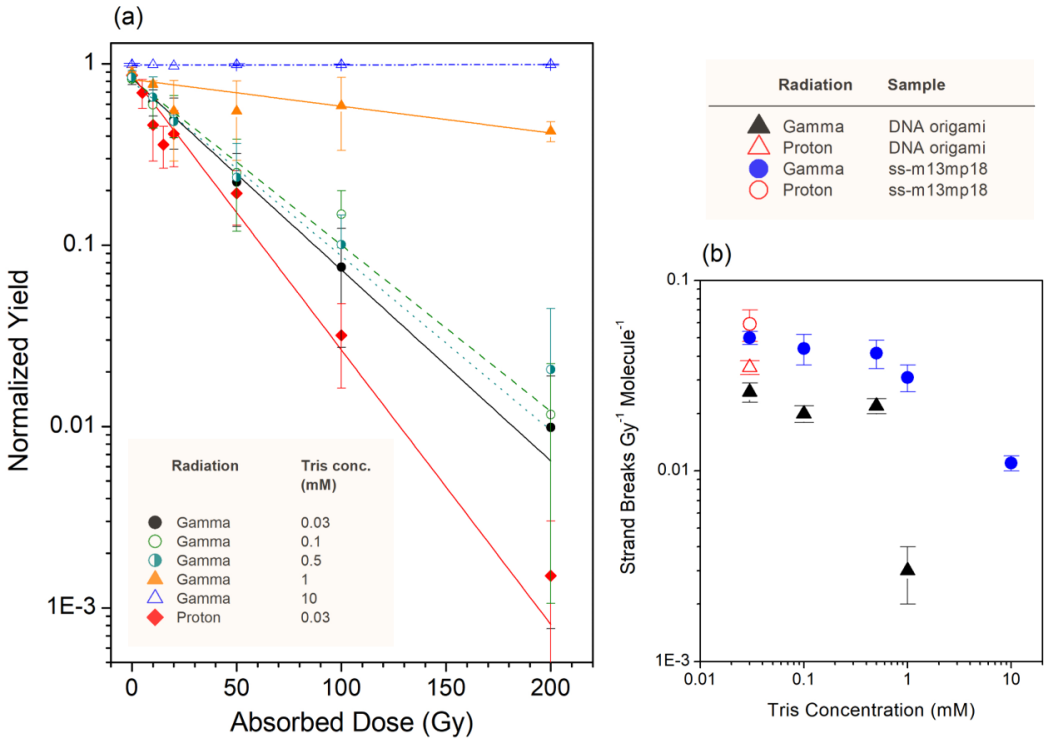

Figure S4 The absorbed dose-dependent decay of the DNA origami scaffold strand with exponential fits to estimate the number of strand breaks in gamma- and proton-irradiated DNA origami solutions with different tris concentrations (shown on the left). At the highest tris concentration shown (10 mM tris, hollow triangles), the line represents the decay of the intact triangle band as the scaffold band does not separate in these conditions. The right panel plots the decay rate of the exponential fits corresponding for both DNA origami and ss-m13mp18.

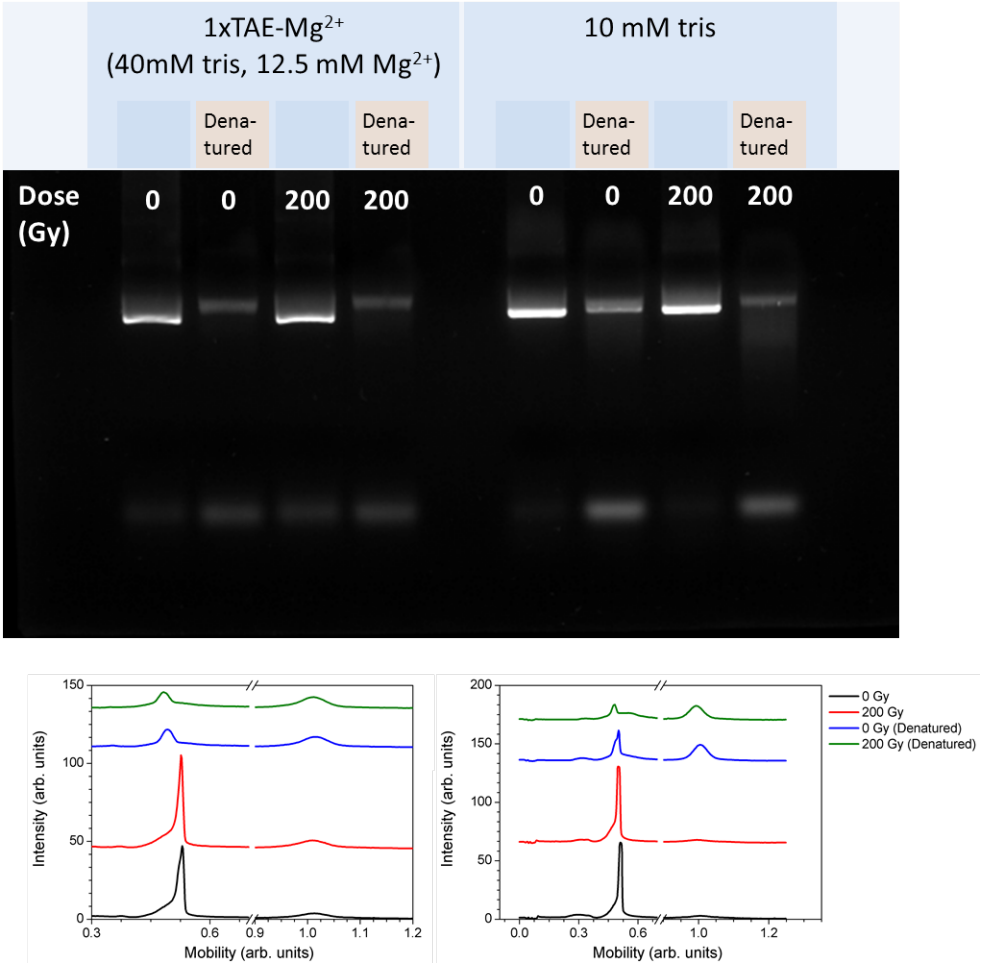

Figure S5 Gel electrophoresis of DNA origami nanostructures in high tris concentrations. The bands show denatured and non-denatured DNA origami nanostructures with and without an absorbed dose of 200 Gy gamma rays.

Table 1 Parameters derived from the exponential fit of the intensity vs. absorbed dose curve from electrophoresis results of DNA origami nanostructures/plasmid DNA irradiated using protons and gamma rays (Fig. S4). Error bars for ssDNA and DNA origami samples are generated from a statistical weighting method implemented on the exponential fit of the absorbed dose dependence of the mean normalized yields.

Radiation	Sample	Scavenger	Scavenger Concentration [S]/ mM	Scavenging Capacity (σ_{OH})*/ 10^5 s^{-1}	μ_{SB}/ scaffold^{-1} Gy^{-1}	R^2	N/ replicates point^{-1}
p^+	Triangle	Tris	0.03	0.45	0.035 ± 0.003	0.993	3
p^+	Triangle	Tris	0.1	1.95	0.030 ± 0.002	0.994	2
γ	Triangle	Tris	0.03	0.45	0.026 ± 0.001	0.996	3-6
γ	Triangle	Tris	0.1	1.95	0.020 ± 0.002	0.985	3
γ	Triangle	Tris	0.5	7.95	0.022 ± 0.002	0.989	2
γ	Triangle	Tris	1	15.5	0.003 ± 0.001	0.910	3
γ	Triangle	Tris	10	150	-	-	2
γ	Triangle	Glycerol	0.1	2.35	0.021 ± 0.004	0.972	2
γ	Triangle	Glycerol	0.5	9.95	0.024 ± 0.003	0.965	3
γ	Triangle	Glycerol	1	19.5	0.018 ± 0.003	0.958	2
γ	dsm13mp18	Tris	0.03	0.45	0.38 ± 0.03	0.998	1
γ	dsm13mp18	Tris	1	15.5	0.33 ± 0.02	0.998	2
γ	dsm13mp18	Glycerol	0.5	9.95	0.34 ± 0.03	0.998	1
p^+	ssm13mp18	Tris	0.03	0.45	0.059 ± 0.011	0.965	1
γ	ssm13mp18	Tris	0.03	0.45	0.050 ± 0.004	0.985	3
γ	ssm13mp18	Tris	0.1	1.95	0.044 ± 0.008	0.930	2
γ	ssm13mp18	Tris	0.5	7.95	0.042 ± 0.007	0.949	3
γ	ssm13mp18	Tris	1	15.5	0.031 ± 0.005	0.951	2
γ	ssm13mp18	Tris	10	150	0.011 ± 0.001	0.989	1
γ	ssm13mp18	Glycerol	0.1	2.35	0.049 ± 0.007	0.948	2
γ	ssm13mp18	Glycerol	0.5	9.95	0.041 ± 0.006	0.960	3

$\sigma_{OH} = k[S]$, residual tris after the buffer exchange is accounted for in these values.

4 Representative AFM images of DNA origami irradiated in various conditions

Fig. S6 to S8 show representative AFM images of DNA origami nanostructures irradiated with gamma rays and 30 MeV protons in H_2O and 0.1 mM tris. The images show minimal change in the triangular structure with absorbed dose in both dry and irradiated solutions. Subjecting the irradiated triangles to some denaturing condition afterwards such as mixing them with pure TAE before AFM imaging may provide some clues with regards to the damage incurred by ionizing radiation. This shows some potential for AFM imaging as a means to quantify radiation induced damage. The particle size (area) distributions on AFM images of "denatured" DNA-origami solutions reveal only partial denaturation when compared to the size distribution in AFM images of pure scaffold DNA and pure triangles. This probably means that it still needs some assistance (e.g. electrophoretic gradient in AGE, heat, or stronger denaturing agents) to ensure complete separation of the scaffold from the staples although additional treatment might also augment the observed damage. Nevertheless, the distribution shifts towards smaller sizes Fig. S7 with high absorbed doses showing some evidence of fragmentation.

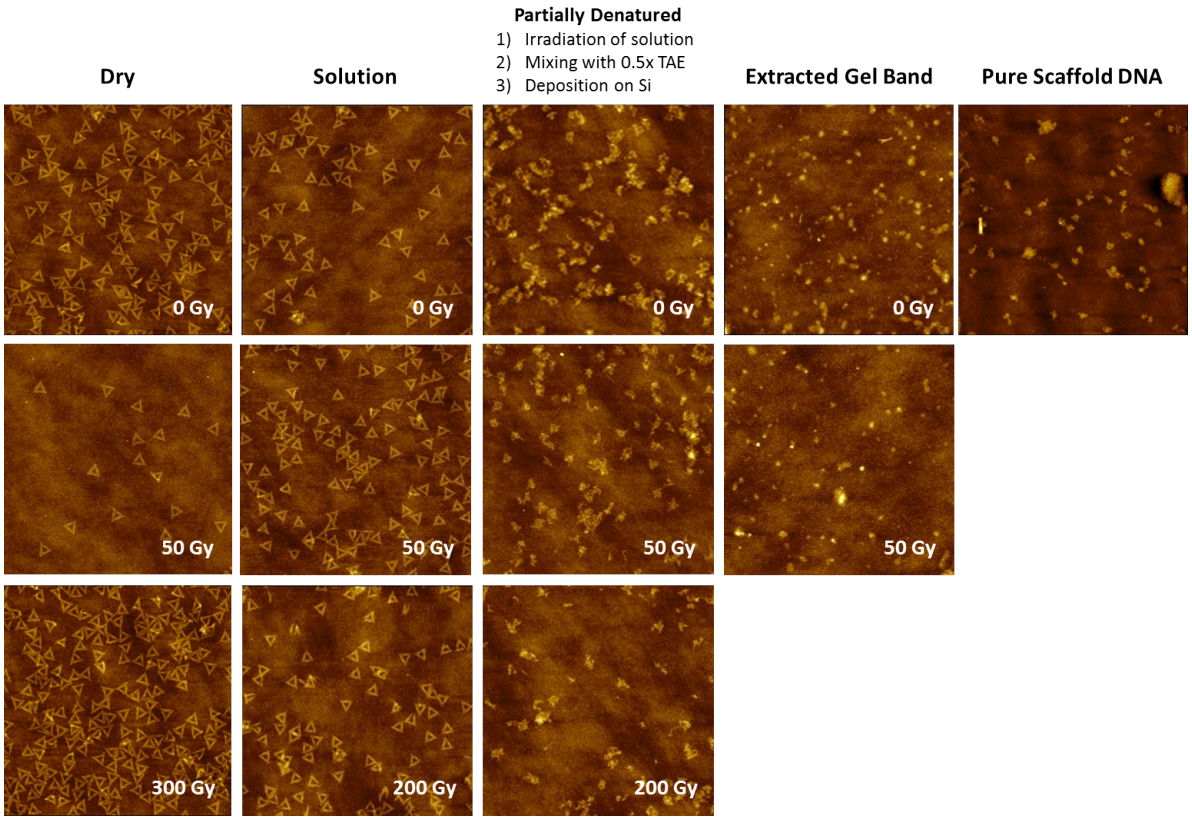

Figure S6 Representative AFM images of gamma-irradiated triangles (50 and 200/300 Gy) and control samples in dry state (1st column), in H_2O (2nd column), and after additional denaturing treatment with 0.5×TAE (3rd column). The images of deposited gel extracts from the corresponding scaffold bands, and an image of the pure scaffold deposited on Si wafer are also shown in the 4th and 5th columns.

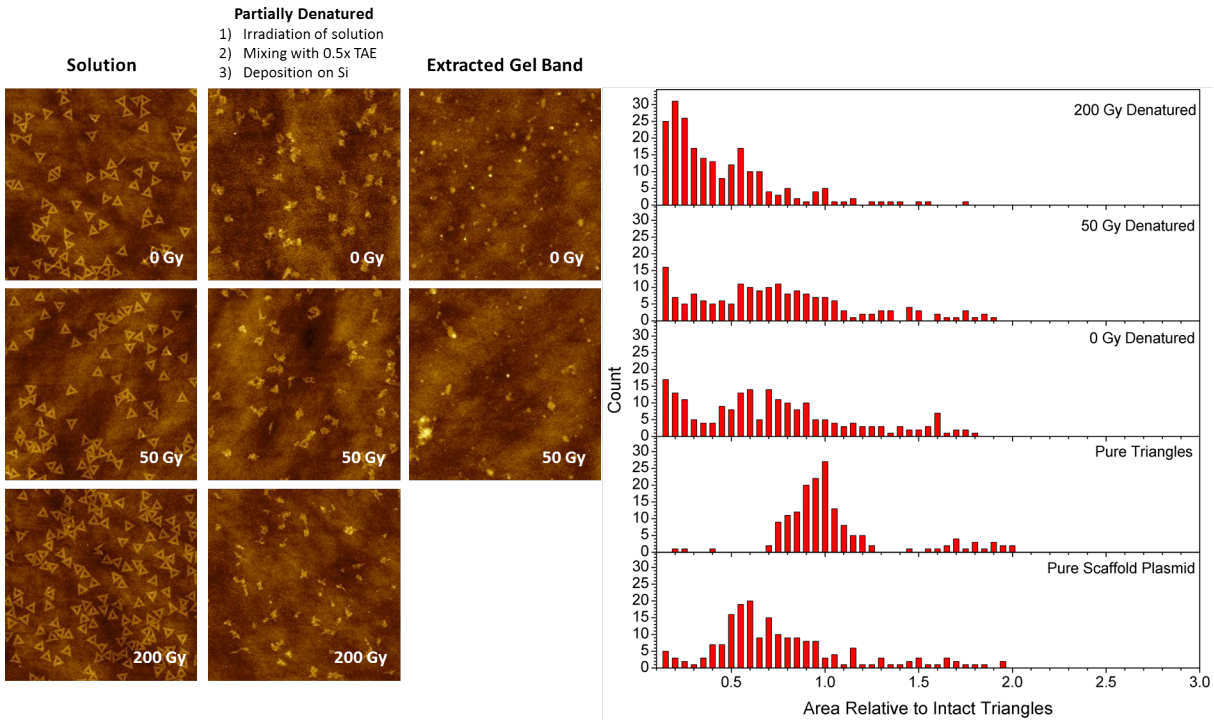

Figure S7 Representative AFM images of gamma-irradiated triangles (50 and 200 Gy) and control samples in 0.1 mM tris (1st column) and after additional denaturing treatment with 0.5xTAE (2nd column). Images of deposited gel extracts from the corresponding scaffold bands are shown in the 3rd column. The particle area distributions of partially denatured irradiated triangles in 1XTAE are shown on the right compared to the particle area distributions of the pure scaffold and pure triangles. The areas were normalized to the average particle area of pure DNA origami triangles

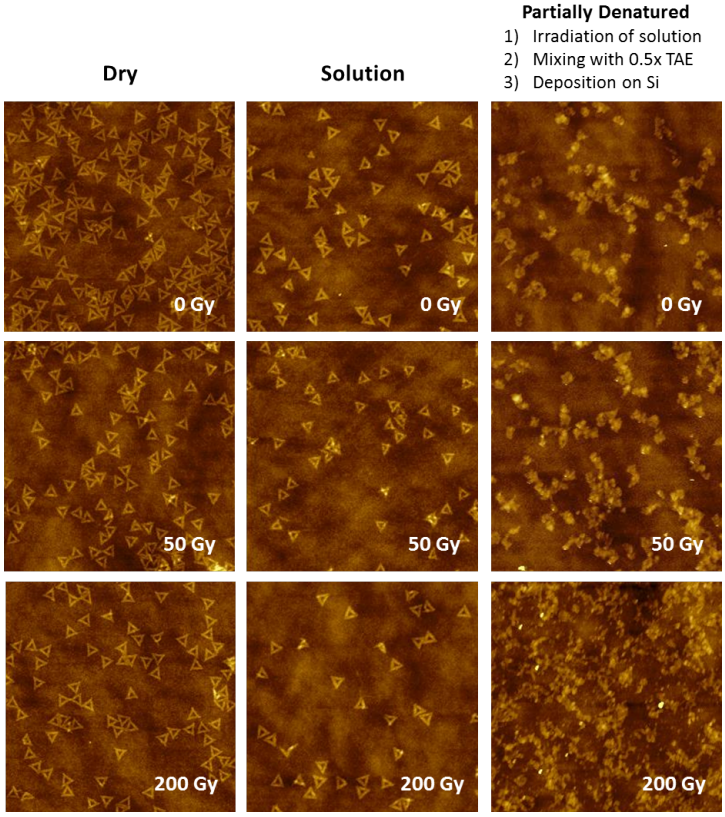

Figure S8 Representative AFM images of proton-irradiated triangles (50 and 200/300 Gy) and control samples in dry state (1st column), in H_2O (2nd column), and after additional denaturing treatment with 0.5xTAE (3rd column).

References

1 C. D. Georgiou, I. Papapostolou and K. Grintzalis, *Nature Protocols*, 2009, **4**, 125–131.

2 R. Cowan, C. M. Collis and G. W. Grigg, *Journal of Theoretical Biology*, 1987, **127**, 229–245.

3 K. P. Brabcová, Z. Jamborová, A. Michaelidesová, M. Davídková, S. Kodaira, M. Šefl and V. Štěpán, *Radiat Prot Dosimetry*, 2019, **186**, 168–171.

4 C. Kielar, Y. Xin, B. Shen, M. A. Kostiainen, G. Grundmeier, V. Linko and A. Keller, *Angew. Chem. Int. Ed.*, 2018, **57**, 9470–9474.

5 Y. Chen, P. Wang, Y. Xu, X. Li, Y. Zhu, Y. Zhang, J. Zhu, G. Huang and D. He, *ACS Appl. Bio Mater.*, 2018, **1**, 1424–1429.